Biosensors and Bioelectronics 189 (2021): 113375

DOI: https://doi.org/10.1016/j.bios.2021.113375

A MoS_2 platform and thionine-carbon nanodots for sensitive and selective detection of pathogens

Emiliano Martínez-Periñán [a‡], *Tania García-Mendiola* [a,b*‡], *Estefanía Enebral-Romero* [a], *Rafael del Caño* [a], *Mariano Vera-Hidalgo* [c], *Manuel Vázquez Sulleiro* [c], *Cristina Navío* [c], *Félix Pariente* [a], *Emilio M. Pérez* [c] *and Encarnación Lorenzo* [a,b,c*]

[a] Departamento de Química Analítica. Universidad Autónoma de Madrid. 28049 Madrid (Spain).

[b] Institute for Advanced Research in Chemical Sciences (IAdChem), Universidad Autónoma de Madrid, Ciudad Universitaria de Cantoblanco, 28049, Madrid (Spain).

[c] IMDEA-Nanociencia, Ciudad Universitaria de Cantoblanco, 28049, Madrid (Spain).

*Corresponding author: tania.garcia@uam.es, encarnacion.lorenzo@uam.es

‡ Both authors contribute equally to this work.

https://doi.org/10.1016/j.bios.2021.113375

ABSTRACT: This work focuses on the combination of molybdenum disulfide (MoS_2) and *à la carte* functionalized carbon nanodots (CNDs) for the development of DNA biosensors for selective and sensitive detection of pathogens. MoS_2 flakes prepared through liquid-phase exfoliation, serves as platform for thiolated DNA probe immobilization, while thionine functionalized carbon nanodots (Thi-CNDs) are used as electrochemical indicator of the hybridization event. Spectroscopic and electrochemical studies confirmed the interaction of Thi-CNDs with DNA. As an illustration of the pathogen biosensor functioning, DNA sequences from InIA gen of *Listeria monocytogenes* bacteria and open reading frame sequence (ORF1ab) of SARS-CoV-2 virus were detected and quantified with a detection limit of 67.0 fM and 1.01 pM, respectively. Given the paradigmatic selectivity of the DNA hybridization, this approach allows pathogen detection in the presence of other pathogens, demonstrated by the detection of *Listeria monocytogenes* in presence of *Escherichia Coli*. We note that this design is in principle amenable to any pathogen for which the DNA has been sequenced, including other viruses and bacteria. As example of the application of the method in real samples it has been used to directly detect *Listeria monocytogenes in* cultures without any DNA Polymerase Chain Reaction (PCR) amplification process.

KEYWORDS. MoS_2, biosensor, CNDs, COVID-19, *Listeria*.

1. Introduction

Pathogens are infectious agents that cause important diseases. Some of the most common pathogens include viruses and bacteria, both vary in many regards, such as virulence, contagiousness, mode of transmission, and infectious dose. In fact, the world is currently facing a global pandemic associated with the SARS-CoV-2, for which virulence and infectious dose data are recently known. Similarly, food-borne diseases caused by pathogenic bacteria (*Escherichia coli, Salmonella enterica*, and *Listeria monocytogenes*) are becoming increasingly worse and causing major public health problems. These pathogenic bacteria can be rapidly spread by the ingestion of contaminated water or food, causing the outbreak of food-borne illnesses, and leading to human diseases and even death (Marušić, 2011; Scallan et al., 2011). In particular, *Listeria monocytogenes* is responsible for causing listeriosis in humans (Hunt et al., 2017) and it is classified as an opportunist dangerous pathogen, especially for high-risk groups of population like babies, pregnant women, elderly and immunosuppressed individuals.

In order to ensure human health and food safety, it is necessary to rapidly and effectively detect the pathogen at all stages (Gehring and Tu, 2011). Hence, the availability of techniques for sensitive and rapid detection of pathogens in complex matrices, such as body fluids and aerosols, and on surfaces is critical to control the spread and treatment of infectious diseases. Up to now, some traditional methods like the bacterial culture counting, immunology, and polymerase chain reaction (PCR) are often applied for the detection of pathogens. In general, the gold standards for pathogen detection are accuracy and reliability methods (Alahi and Mukhopadhyay, 2017; Law et al., 2015; Lazcka et al., 2007; Malorny et al., 2003). However, they possess the short comings of being time consuming and complicated, which is unsuited to rapid detection.

Recently, biosensors have been recognized as popular devices for detecting pathogens, with excellent properties, such as simplicity, speediness, and sensitivity (Gehring and Tu, 2011). These devices are an excellent alternative to traditional methods. They can be broadly distinguished as immunosensors or DNA-based biosensors. The use of one or the other will depend on the stage of the infection and the availability of antibodies and DNA

sequence data, such as viral DNA, toxin-producing genes, as well as species- and strain-selective genes.

In previously reported DNA biosensors, different detection methods have been applied, including colorimetric, fluorescence, electrochemical, chemiluminescence and electrochemiluminescence. Among these methods, electrochemical has been proven to be well-suited to simple and rapidly detect DNA sequences and several electrochemical biosensors for pathogen detection have been reported (Cesewski and Johnson, 2020). However, some aspects of these biosensors still need to be improved. Therefore, the development of new simple, inexpensive and sensitive electrochemical biosensors for pathogen DNA detection continues to be a research topic of great interest and application. To this end, in recent years, the use of nanomaterials in biosensors fabrication have become a research hotspot due to their attractive electrochemical and photoelectric properties, laying the foundation for signal amplification methods. In particular, recently, the combination of different nanomaterials with specific functions (such as facilitate the immobilization of the recognition biomolecule or amplify the signal response) have been successfully applied to the design of biosensors, bringing down the detection limit (Rohaizad et al., 2021). Among the different types of nanomaterials, a promising one as a sensing interface is molybdenum disulphide (MoS_2). Due to its unique covalent bonding properties it has been increasingly used to develop electrochemical biosensors (Lin et al., 2020; Nie et al., 2020). Also combined with other nanomaterials in order to achieve lower detection limits (Dutta et al., 2018; Yang et al., 2017; Pen et al., 2018; Su et al., 2015).

In electrochemical DNA biosensors, the hybridization between the probe and the target DNA is detected by the different binding affinity of single strand DNA (ssDNA) and double strand DNA (dsDNA) for a redox active molecule, such as fenothiazines (García-Mendiola et al., 2016; García-Mendiola et al., 2020). Based on these previous works, here we have modified carbon nanodots with a fenothiazine, thionine, endowing them with redox properties in order to be employed as redox indicators of DNA hybridization event. Compared to other carbon-based nanomaterials, carbon nanodots (CNDs) have emerged recently due to their higher solubility and biocompativility. In addition, they do not require of heavy metal or contaminant solvents for the synthesis. In fact, they are prepared from compounds abundant in the nature and their surface can be easily modified through various post-synthetic procedures, endowing them with specific functions (Rigodanza et al., 2018). In the present work, by combining the thionine-modified carbon nanodots (Thi-

CNDs) synthetized with the 2D nanomaterial, MoS_2, we developed an electrochemical biosensor for the sensitive and selective detection of pathogen DNA sequences with a broad applicability.

MoS_2-PtPd has been recently used as substrate for loading of an apatamer to recognize microcystin-LR. To increase the sensitivity of the aptasensor, Wu et al. developed an indirect method for detection through synthetizing and utilizing a zeolitic imidazole framework-8-thionine-Au as signal material (Wu et al., 2020). Our strategy of supporting thionine on carbon nanodots is simpler and used for first time in this work.

An electrochemical immunosensing platform based on thin-layer MoS_2 and thionine (MoS_2-Thi) composites was constructed for the sensitive and rapid detection of zearalenone (ZEA) in human biofluids. To improve the performance of the electrochemical immunosensor, Pt NPs were conjugated to antibodies (Jiang et al., 2019).

In order to assess the applicability of our device to the detection of pathogen in general, as case study, we have applied the biosensor to the detection of DNA sequences of SARS-CoV-2 virus and *Listeria monocytogenes* bacterium. In addition, the biosensor allows both samples to be quantified with a detection limit of 1.01 pM and of 67.0 fM for the virus and bacterium, respectively. As can be seen in Scheme 1, MoS_2 nanosheets are drop-casted onto a disposable screen-printed carbon electrode. The probe-target DNA hybridization is conducted to detect specific DNA sequences from SARS-CoV-2 or *Listeria monocytogenes* genes*,* by immobilizing the corresponding thiolated DNA probe on the MoS_2 surface. Due to the unique properties of Probe/MoS_2 as the sensing interface and Thi-CNDs as the hybridization redox indicator, sensitive detection of two important pathogens, the SARS-CoV-2 and the *Listeria* is achieved. The utility of the developed biosensor in practical cases has been proved by applying it to the detection and quantification of genomic DNA samples extracted from *Listeria monocytogenes* culture. We have focused the application on *Listeria* due to the difficult and special conditions for handling and access to real samples from coronavirus disease 2019 (COVID-19) patients.

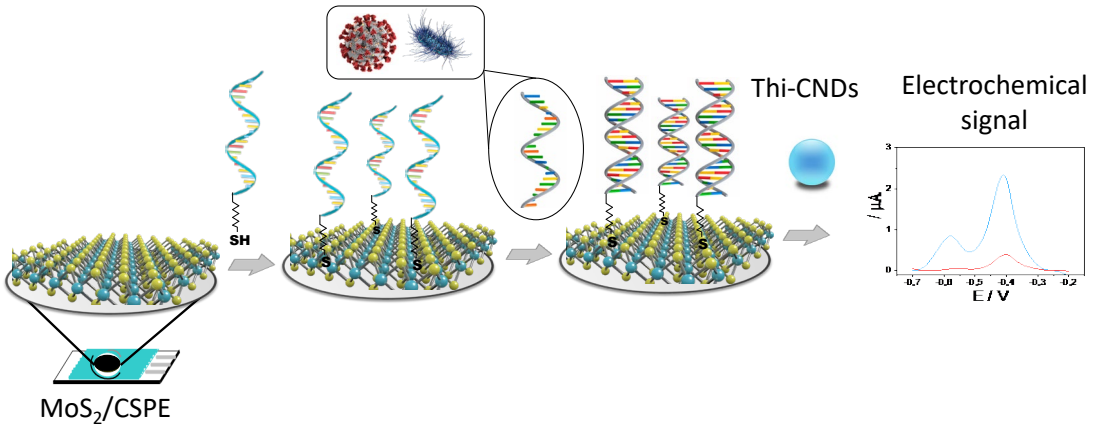

Scheme 1. Biosensor development.

2. Experimental

2.1. Materials and apparatus

Materials and apparatus used in this work are described in the Supporting information (SI).

2.2. Thionine functionalized Carbon nanodots (Thi-CNDs) synthesis

Thi-CNDs were directly synthesized as follows: 87 mg L-arginine, 72 mg Thionin acetate salt, 86 µL 3,3'-diamino-N-methyldipropylamine and 100 µL Milli-Q water were irradiated in a microwave system at a constant temperature of 235 ºC and a maximum pressure of 20 bar during 180 s. Then, the blue solid obtained was dissolved in 10 mL of ultra-pure water and filtered using 0.1 µm porous filter. The suspension was dialyzed in a 0.1-0.5 kDa dialysis membrane for 1 week. The final concentration of as prepared Thi-CNDs was 2.83 mg mL^{-1}. The resulting solution was stored at 4ºC. CNDs without thionine were also synthesized following the same procedure (except the addition of thionine acetate) as were reported in the literature (Guerrero-Esteban et al., 2021).

2.3. Biosensor development

Firstly, CSPE electrodes were modified by drop casting 10 µL of a molybdenum disulfide (MoS_2) stock solution and allowed to stand overnight (MoS_2/CSPE). Afterwards, 10 µL of 10.0 µM thiolated synthetic DNA sequences ($Probe_{List}$-SH or $Probe_{CoV}$-SH) were deposited on the MoS_2/CSPE and it was kept at room temperature in a humidity chamber

for 24 hours. Finally, it was soaked in Milli-Q water for 30 min. The resulting modified electrodes are named as $Probe_{List}$-SH or $Probe_{CoV}$-SH/ MoS_2/CSPE.

2.3.1. Hybridization and electrochemical detection of Listeria and SARS-CoV-2

The $Probe_{List}$-SH or $Probe_{CoV}$-SH/ MoS_2/CSPE was hybridized in 10 mM phosphate buffer (pH 7.0) with 0.4 M NaCl for 1 h at 40 ºC with 10 µL of the analyte solution, which may content a totally complementary or non-complementary synthetic sequence corresponding to *Listeria* or SARS-CoV-2. In the case of *Listeria* sensing, genomic DNA extracted from *Listeria monocytogenes* culture was also used. Then, Thi-CNDs were accumulated on the dsDNA layer formed on the electrode surface by immersing the modified electrode in 0.1 M phosphate buffer pH 7.0 (PB) containing Thi-CNDs (0.280 mg mL^{-1}) and cycling the potential from -0.70 to -0.15 V (100 scans) at 100 mV s^{-1}. Finally, the electrodes were rinsed with sterile water, placed in 0.1 M PB pH 7.0 and differential pulse voltammograms (DPV) were immediately recorded at a scan rate of 10 mV s^{-1}.

2.3.2. Detection of Listeria in genomic DNA extracted from Listeria monocytogenes culture.

Genomic DNA was extracted from the cultured *Listeria monocytogenes* as described in detail in the SI. Then, genomic DNA samples were denatured by heating until 100 ºC for 15 minutes followed by rapid cooling (Pang et al., 1995). 10 µL of denatured sample were diluted to a final volume of 60 µL with 10 mM phosphate buffer (pH 7.0) with 0.4 M NaCl. The final total DNA concentration in this diluted sample was of 52.0 ng μL^{-1}(1.67 $\times 10^8$ CFU mL^{-1}), determined with the NanoDrop spectrophotometer, which corresponds to 0.45 pg μL^{-1}or 0.58 nM of a sequence of InIA gen. 10 µL of this sample were deposited on the $Probe_{List}$-SH/ MoS_2/CSPE and were hybridized for 1 h at 40 ºC. Finally, Thi-CNDs were accumulated on the hybridized DNA layer as we described above and differential pulse voltammograms (DPV) were recorded. Current was measured at -0.4 V (higher peak) of the accumulated Thi-CNDs.

3. Results and discussion

3.1. Synthesis and characterization of MoS_2

Few layers colloids of MoS_2 were obtained through liquid-phase exfoliation as it is explained in detail in the SI. The resulting olive color dispersion was characterized by UV-Vis and Raman spectroscopy (Figure S1) confirming the 2H-polytipe MoS_2. The UV-Vis dispersion of the colloids showed a significant scattering of the sample and the typical bands associated to A and B excitons of MoS_2 (624 and 685 nm). Moreover, C and D exciton bands, that correspond to higher energy transitions from the band edges, are observed at 488 and 411 nm respectively (Giovanelli et al., 2017). Raman spectrum of the powder MoS_2 are dominated by the characteristic E^1_{2g} (385 cm^{-1}) and A_{1g} (405 cm^{-1}) modes (Figure S1B) (Li et al., 2012).

3.2. Synthesis and characterization of Thionine functionalized Carbon Nanodots (Thi-CNDs)

Thi-CNDs were synthesized following a similar procedure with variations to that described by F. Arcudi et al, as is explained in detail in the experimental section (Arcudi et al., 2016; Rigodanza et al., 2018).

The TEM image (Figure 1A) shows Thi-CNDs as quasi-spherical nanoparticles. The size distribution of Thi-CND, estimated by measuring the average size of around 120 Thi-CNDs (see histogram at Figure S2), indicates a mean size of 3.1 nm ranging from 1.5 to 5.0 nm in diameter.

Figure 1B shows the FT-IR spectrum of Thi-CNDs, besides CNDs and thionine acetate spectra. In the thionine acetate spectrum, the band at 3336 cm^{-1} is associated to primary amine (N-H stretch asym) while the band at 3147 cm^{-1} is due to the N-H stretch sym. Bands around 2972 and 1617 cm^{-1} are assigned to the acetate anions of the thionine salt and to the N-H bonding, respectively. CNDs present the characteristic stretching band of OH and NH_2 as a broad band centered at 3436 cm^{-1}, the bands observed around 2930 cm^{-1} derive from the C-H bond stretching vibration. C=O stretching vibrations appear at 1644 cm^{-1}. The small band at 1562 cm^{-1} is ascribed to the C=N stretching, while the bands at 1457 cm^{-1} and 1384 cm^{-1} are related with C-N bonds. The 1071 cm^{-1} bands correspond to the C-O stretching vibrations. The FT-IR spectrum of Thi-CNDs is quite similar to that of CNDs; however, the wide band at 3436 cm^{-1}, which is consistent with the presence of a great number of amine groups due to the thionine, and the increase of the band at 1617 cm^{-1} also associated with thionine, suggest thionine modification of CNDs. Although these results are not conclusive, they indicate small compositional changes that agree well with the presence of thionine.

The UV-Vis spectrum (Figure 1C) of Thi-CNDs (curve a, blue) shows a great absorption peak at 285 nm, which can have various contribution as the π-π* transition of the conjugated C=C units associated with the carbon dots (curve b, red) and the π – π* transition of a phenothiazine ring. The peak ascribed to the thionine covalently linked with the CNDs is centered at 603 nm, close to the maximum at 598 nm of thionine acetate solution (curve c, black) attributed to H-type dimers of the dye and/or a vibrational band assigned to the n–π* transitions of the C=N bond (Jiang et al., 2015). The aggregate shoulder (559 nm) shows a considerably increase. Other feature that is worth to highlight is a great light scattering because of the nanomaterial suspension compared with the clear solution of thionine. The absorption bands at 283 and 318 nm are attributed to the π – π* transition of a phenothiazine ring and the n– π* transition of an amine group, respectively (Krzyszkowska et al., 2017). As can be deduced from UV-Vis spectra, CNDs have been effectively functionalized with thionine, obtaining a new material with important differences in the absorption spectra.

Cyclic voltammograms (CVs) of Thi-CNDs were carried out using a carbon screen-printed electrode (CSPE) and compared to CVs of CNDs and thionine (Figure 1D). Two reversible redox process at formal potential of -0.38 V and -0.54 V *vs.* Ag/AgCl are observed (curve a, blue). Each of these processes exchanges one electron (obtained by Tafel plot). No redox process is observed at CNDs solution (curve b, red), which indicates that no faradaic process occurs. Thionine (curve c, black) shows the characteristic redox couple at a formal potential of -0.38 V. This process involves two electrons. These results evidenced again the thionine modification of CNDs, suggesting that the reaction is not a simple adsorption of the colorant over the CNDs but rather that it has been embedded in the nanomaterial structure.

Figure 1E and F shows XPS spectra of the main features of Thi- CNDs (curve a, blue), CNDs (curve b, red) and thionine acetate (curve c, black): the N 1s core level and S 2p. All the spectra have been normalized in intensity to better observe the small changes in shape and chemical shifts. For the N 1s peak, there is mainly one component in all samples: in those cases where there is more than one type of N, the components are too close and cannot be discriminated. But the presence of S on the Thi-CNDs sample and chemical shift that the N 1s of CNDs suffer of 0.2 eV towards higher binding energies, points towards a successful anchoring of the thionine on the CNDs.

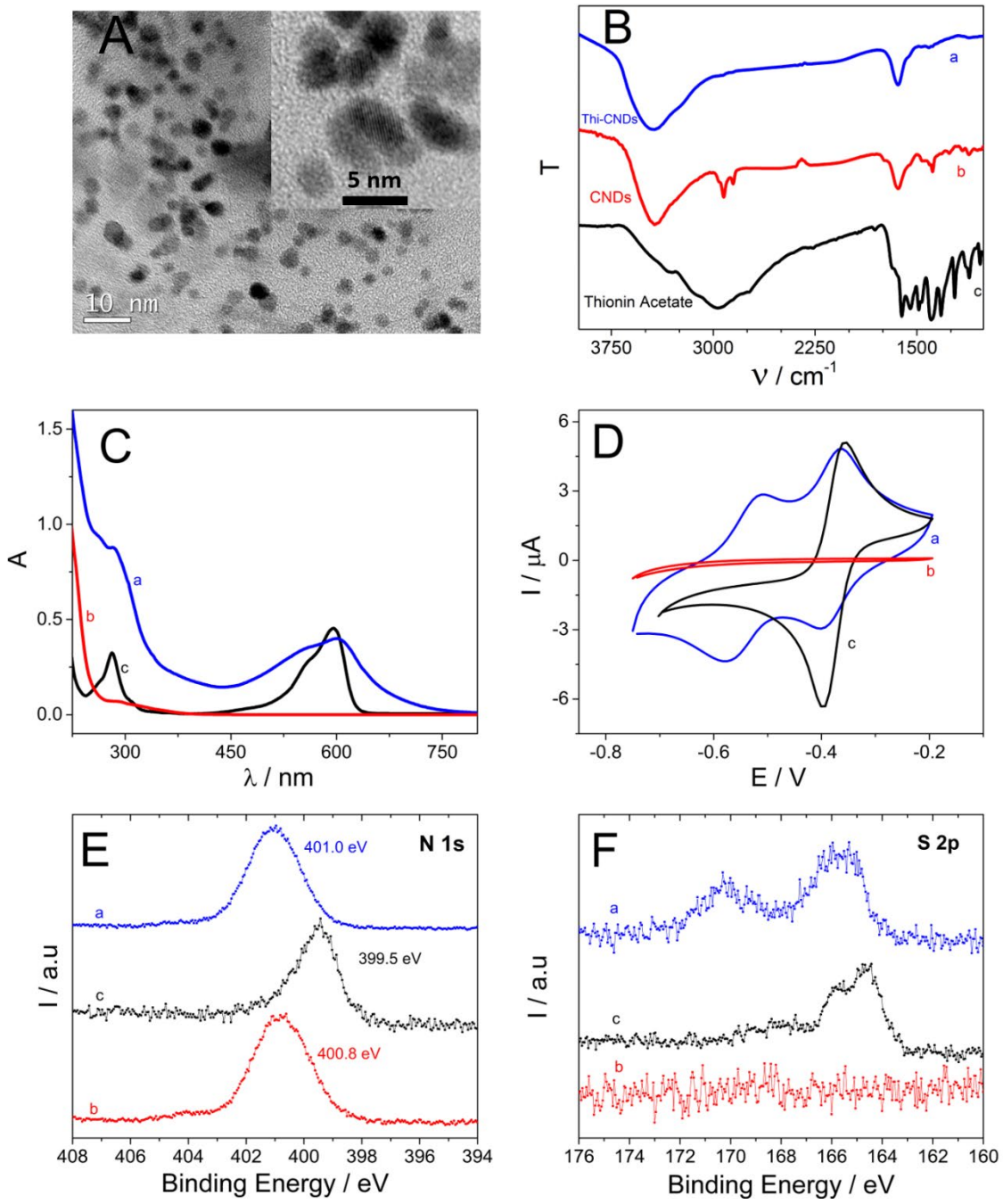

Figure 1. (A) Thi-CNDs TEM micrograph. (B) FT-IR and (C) UV-Vis spectra and (D) Cyclic voltammetry in 0.1 M PB buffer pH 7 at 0.01 V s^{-1} of 0.283 mg/mL Thi-CNDs (curve a, blue), 0.283 mg/mL CNDs (curve b, red) and 50 μM Thionine acetate (curve c, black). (E) XPS spectra core levels of N 1s and (F) S 2p of Thi-CNDs (curve a, blue), CNDs (curve b, red) and thionine acetate (curve c, black).

3.3.DNA and Thi-CNDs Interaction

We have studied the Thi-CNDs interaction with DNA by combining spectroscopic and electrochemical studies as is explained in detail and discussed in the SI. The results point out to a strong interaction between the Thi-CNDs and DNA, being stronger with ds than with ssDNA, and therefore the potential utility of Thi-CNDs as electrochemical indicator of the hybridization event.

3.4. Development and Characterization of the pathogen biosensor.

After electrode modification with MoS_2 by drop casting (see Scheme 1), the corresponding DNA capture probe, a single stranded DNA sequence totally complementary to the target analyte, modified at 5′-end with an hexalquilthiol (Probe-SH) (Catalán-Gómez et al., 2020) is immobilized on the MoS_2. The organic molecules with -SH group tend to repair or eliminate S vacancies (VS) of the MoS_2 lattice, resulting in the molecular functionalization with the substrate (Chen et al., 2018; Jariwala et al., 2014; Tuxen et al., 2010; Wang et al., 2012). Within the framework of developing an approach with broad applicability, as case study, we choose two different pathogens as target analyte: the SARS-CoV-2 virus that is causing the pandemic that is currently suffering the world, and *Listeria monocytogenes*.

The biosensing platform were characterized by scanning electron microscopy (SEM), energy dispersive X-ray spectroscopy (EDX), Raman spectroscopy, Cyclic Voltammetry (CV), X-Ray diffraction (XRD) and X-ray photoelectron spectroscopy (XPS).

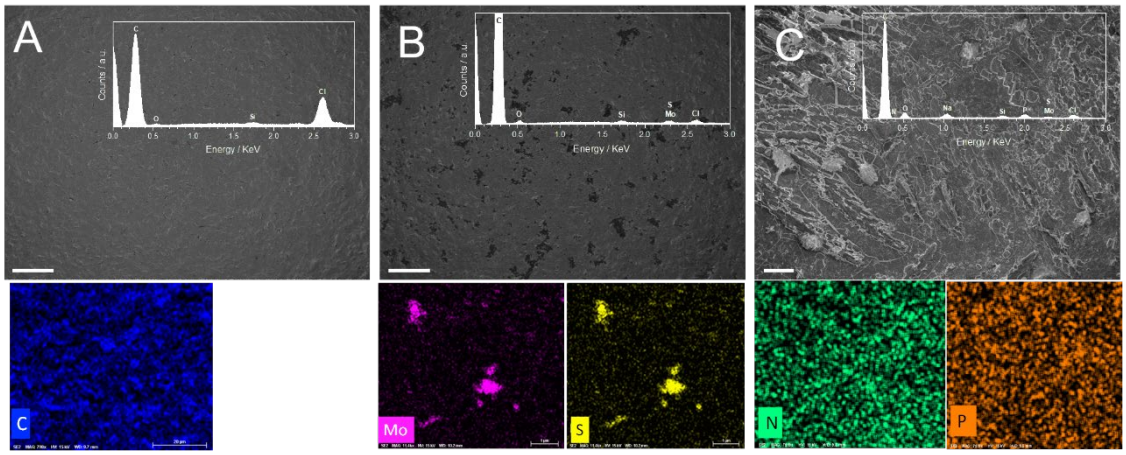

Figure 2. SEM and EDX images (inset and bottom) of a magnification of (A) CSPE (B) MoS_2/CSPE and (C) Probe-SH/MoS_2/CSPE. The scale bar corresponds to 100 µm.

The SEM image of the bare electrode (see Figure 2A) shows a rough surface that, according to the EDX spectrum, is mainly composed of carbon. After MoS_2 modification (Figure 2B) the electrode surface appears covered by MoS_2 layers and the EDX spectrum confirms the presence of Mo and S (inset and bottom part of Figure 2B). The morphology of the prepared electrodes was also characterized by Atomic Force Microscopy (AFM). Bare CSPE showed a homogeneous rough surface and height (Figure S7A). Similar profile is observed after the MoS_2 modification of the electrode with the singularity of smoother areas due to the presence of the MoS2 flakes (Figure S7B).

Immobilization of the thiolated DNA probe on the MoS_2 modified electrodes (Probe-SH/ MoS_2/CSPE) was also assessed by EDX, AFM, Raman, CV, XRD and XPS. As can be seen in Figure 2C, after DNA probe immobilization, in addition to the EDX spectrum of MoS_2, it is possible to observe N and P that probably come from the DNA immobilized on the MoS_2/CSPE. From the AFM images (Figure S7C) it is clear the immobilization of the thiolated DNA probe increased the electrode roughness creating small height variations in its surface. The RAMAN spectra (Figure S8A) show that bare electrode (black line) presents the characteristic D and G bands at 1359 and 1596 cm^{-1} of the carbon forms (Díez Tascón, 2007) in addition to a broad and not very intense band at 2700 cm^{-1} (G band) typically present at carbonaceous solids with low structural order. After MoS_2 adsorption (red line), two new signals at 383 and 409 cm^{-1}, which we assign to the active Raman modes of first order E^1_{2g} and A_{1g} from the semiconductor polymorph 2H-MoS_2, appear (Fan et al., 2015). After the probe immobilization (blue line), a new band at about 2719 cm^{-1}, ascribed to vibrations of thymine, adenine and guanine, appears (dos Santos et al., 2016).

The CV response of Thi-CNDs at a CSPE, a MoS_2/CSPE and a probe-SH/ MoS_2/CSPE, (see Figure S8B) shows the characteristic redox couples, previously ascribed to the oxidation/reduction of the Thi-CNDs. However, as one would expect, the presence of MoS_2 flakes causes an increase in the peak current without shift in the formal potentials. When the electrode is modified with the probe (probe-SH/ MoS_2/CSPE), as we described above for ssDNA/CSPE, only the peak of Thi-CNDs at around -0.4 V is well defined. These results are compatible with the immobilization of the capture probe on the MoS_2/CSPE.

Figure S9 displayed the XRD patterns of CSPE, MoS_2/CSPE and Thi-CNDs/dsDNA/MoS_2/CSPE. Clearly, after the modification of the electrode with MoS_2 it was observed a new peak from the XRD at $2\theta = 14.3°$ (red curve, Figure S9), which was

attributed to the characteristic peak of MoS_2 (002) (Liu et al, 2014; Quiros-Ovies et al, 2020). In addition, the further modification of Thi-CNDs/dsDNA/MoS_2/CSPE basically retains the position of the diffraction peaks of MoS_2, while the intensity becomes weaker. The later decrease could be attributed from the partial blocking of the MoS_2 dispersion caused by the incorporation of new fragments in the electrode.

MoS_2 XPS spectrum is noisy (Figure S10), due to the low signal, but the main features are clearly distinguishable. On the region with the Mo 3d and S 2s is shown, where two clear chemical states for the Mo can be seen: the Mo^{4+}, corresponding to MoS_2, and an important contribution of Mo^{6+}, most probably Mo oxide. The immobilization of DNA capture probe on the MoS_2 is demonstrated by the presence of N (as well as P and Na, see survey spectra of Figure S11).

3.5. Detection of pathogens

We applied the biosensor to the detection of two different pathogens in order to assess its broad applicability: *Listeria monocytogenes* and SARS-CoV-2. In the case of SARS-CoV-2 we selected ORF1ab, since it is employed as genetic target in the gold standard technique (the RT-PCR) currently used to detect infection caused by this virus. All the 25 and 28-base oligonucleotide sequences used in this work are listed in Table 1. The DNA sequences comprises the DNA probes (single stranded sequences, totally complementary to the corresponding target analyte, modified at 5′-end with an hexalquilthiol; denoted as $Probe_{List}$-SH and $Probe_{CoV}$-SH for *Listeria* and SARS-CoV-2, respectively), the target sequences (specific sequence from *Listeria monocytogenes* bacteria and SARS-CoV-2 ORF1ab gene, denoted as $Listeria_C$ and CoV_C, respectively) and a non-complementary sequence (denoted in the text as $Listeria_{NC}$ or CoV_{NC}). Besides, genomic DNA samples extracted from cultured *Listeria monocytogenes* and *Lactobacillus rhamnosus* were also used, the latter as a control.

Table 1. DNA sequences used in this work.

Pathogen	Type of sequence	Oligonucleotide sample (5´to 3´)	Named
Listeria (InIA gen)	Probe	SH- CCTAGCAGGTCTAACCGCACTCACT	$Probe_{List}$-SH
	Complementary	AGTGAGTGCGGTTAGACCTGCTAGG	$Listeria_C$
	Non-commplementary	GACTCACTATTCCGACAACATCGAA	$Listeria_{NC}$
SARS-CoV2 (ORF1ab)	Probe	SH- CCATAACCTTTCCACATACCGCAGACGG	$Probe_{CoV}$-SH
	Complementary	CCGTCTGCGGTATGTGGAAAGGTTATGG	CoV_C
	Non-commplementary	CAGGTGGAACCTCATCAGGAGATGC	CoV_{NC}
Escherichia coli	Interferent	TGCCGCTCATCCGCCACATATCCTG	E. Coli

Pathogen detection was based on the hybridization of each analyte sequence either from the open reading frame (ORF1ab) of SARS-CoV-2 (CoV_C) or InIA gen of *Listeria monocytogenes* ($Listeria_C$) with the corresponding capture probe immobilized on the Mo_2S modified electrode surface (as it is explained in detail in the experimental section) under optimal conditions. Hybridization time, temperature and pH were optimized and best results were found for 1 h at 40ºC using 10 mM phosphate buffer (pH 7.0) with 0.4 M NaCl. The synthetized Thi-CNDs were accumulated (by potential cycling) on the dsDNA layer formed on the biosensor surface after hybridization and employed as electrochemical indicators of the hybridization event. Electrochemically driven accumulation allows a properly control of the process (García-Mendiola et al., 2016).

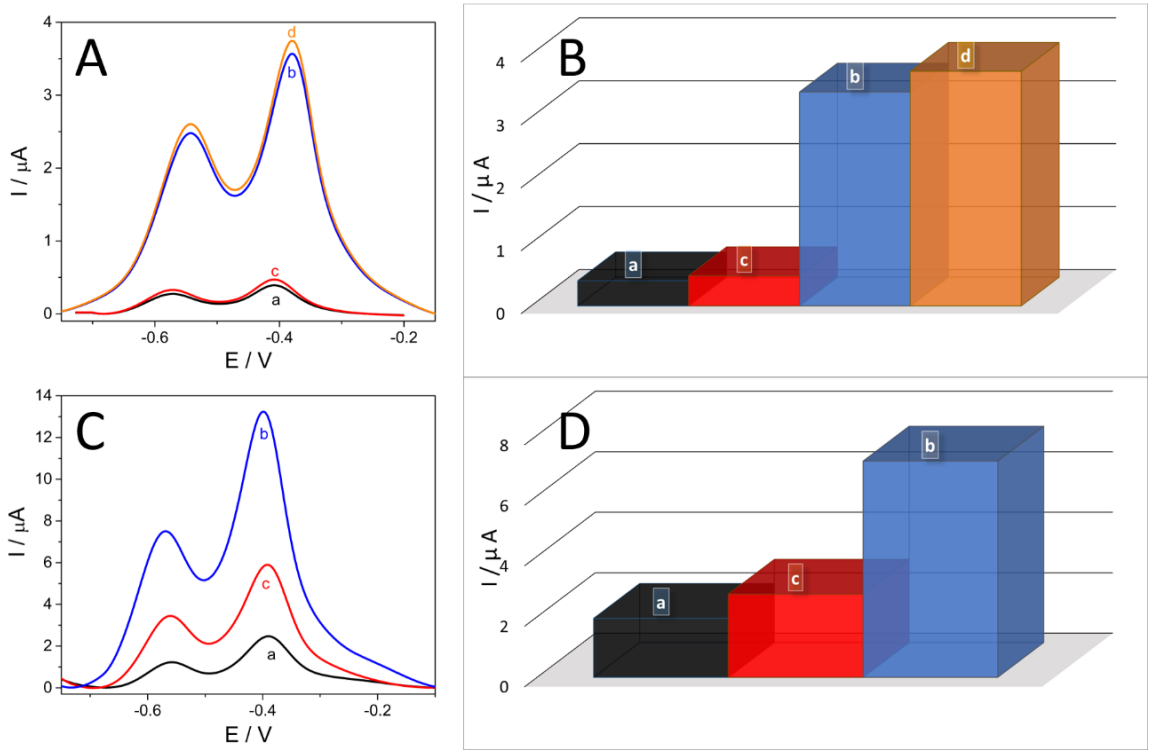

Figure 3. DPVs (A, C) and bare diagrams (B, D) of the peak current (peak 2) of Thi-CNDs accumulated on a Probe-SH/ MoS_2/ CSPE before (curve a, black) and after hybridization with 100 pM: complementary (curve b, blue), $Listeria_c$ (A, B) or CoV_C (C, D), non-complementary (curve c, red), $Listeria_{Nc}$ (A, B) or CoV_{NC} (C, D) and a mixture of complementary sequence of *Listeria* and *Escherichia coli* in the same concentration (curve d, orange) in PB 0.1 M pH 7.0. Scan rate: 10 mV s^{-1}.

Figure 3 shows the DPVs recorded in 0.1 M PB pH 7.0 at the corresponding Probe-SH/ MoS_2/ CSPE before (background) and after hybridization with the targets: complementary *Listeria* ($Listeria_c$) or SARS-CoV-2 (CoV_C) and non-complementary *Listeria* ($Listeria_{Nc}$) or SARS-CoV-2 (CoV_{NC}) sequences, the latter used as control, and subsequent accumulation of the Thi-CNDs. It can be seen a significant enhancement in the electrochemical signal after hybridization with the complementary sequence (more than eight-times higher than the obtained for the probe in the case of *Listeria)*, while a very small change is noted after hybridization with the non-complementary. This signal difference allows to confirm the presence of the pathogen.

The response (at -0.4 V) increases gradually on increasing the analyte concentration (Figure S12 and S13) and fits to a linear equation (Y = 1.34 log [$Listeria_C$] + 5.85; R = 0.9979 and Y = 0.71 log [CoV_C] + 5.23; R = 0.9898). Values are the average of three

determinations with a reproducibility of 97%. The detection and quantification limits (calculated as the probe signal plus 3 and 10 times the standard deviation divided by the slope of the calibration curve) were found to be 67.0 fM and 72.4 fM, for *Listeria* and 1.01 pM and 1.18 pM, for SARS-CoV-2.

The selectivity of the biosensor was assessed from its response to 100 pM *Listeria* in presence of the same concentration of *Escherichia coli* (E. coli), usually present together with *Listeria*. The biosensor response appears to be unaffected by the presence of *E. coli* (Figure 3 A, B), demonstrating the absence of any cross-interference. The reproducibility of the method was estimated from the response of three devices prepared using the same protocol to 1.0 nM analyte sequence. The relative standard deviation (RSD) was calculated to be 3.6 %. Repeatability of the biosensor was also evaluated by measuring 5 times the biosensor response. In this case the RSD was found to be 1.0 %.

The developed biosensor compared well with other similar DNA biosensors previously described for pathogen detection (see SI Table S1). The detection limit is comparable or even better than those reported in the literature. Moreover, the proposed method is simpler and do not require laborious development steps.

3.5.1. Bacteria detection in cultured *Listeria monocytogenes*.

The applicability of the as-developed device was demonstrated by direct detection of *Listeria* in genomic DNA samples extracted from cultured *Listeria monocytogenes,* without PCR amplification process. The experimental details of genomic DNA extraction and *Listeria* detection are described in the SI and in the experimental section, respectively. The biosensor response to *Listeria* is 40 times higher than those obtained for the probe (Figure S14A) and increases on increasing sample concentration from 52.0 to 313 ng μL^{-1} (Figure S14B). A sample extracted from cultured *Lactobacillus rhamnosus,* used as control, gives a biosensor response that is approximately half of the signal corresponding to *Listeria*. Although the difference is enough to be distinguished from the *Listeria* signal, we believe that this relatively high response to *Lactobacillus* is due to the whole extracted DNA from the culture is detected rather than a specific sequence from a gen.

We calculated the concentration of the genomic DNA in the samples directly by introducing the biosensor response to the whole DNA concentration (52.0 ng μL^{-1}determined from NanoDrop spectrophotometer), which theoretically would correspond to 0.58 nM InIA gen, in the calibration plot (Figure S12 B). A concentration of 0.56 ±

0.02 nM InIA gen is obtained, which agrees well with expected. The results demonstrate the proposed biosensor can be used for practical applications and has a great potential as an alternative to the classical methods for detection and quantification of a pathogen without the need of DNA PCR amplification.

4. Conclusions

We developed a simple and efficient electrochemical biosensor based on the interaction between a single stranded oligonucleotide (Probe-SH) and MoS_2 flakes deposited on CSPE combined with Thi-CNDs. The method was applied as a fast and precise screening method for the direct detection of two different pathogens: the SARS-CoV-2 virus and *Listeria* bacterium. The bacterium was detected in samples extracted from cultured *Listeria monocytogenes* without any DNA PCR amplification process. The design is in principle applicable to any pathogen for which the DNA (or fragments of) has been sequenced. A wide range of applications of this type of biosensor is foreseen in the selective and sensitive detection of both viruses and bacteria. Their fabrication and measuring protocols are simple, economical, and non-time consuming. It has a huge potential for greatly simplifying the development of portable food control systems.

Acknowledgements

Authors thank the financial support from the Comunidad de Madrid (NANOAVANSENS, S2013/MIT-3029, MAD2D-CM Program, S2013/MIT-3007 and 2017-T1/BIO-5435), Ministerio de Economía, Industria y Competitividad (CTQ2015-71955-REDT (ELECTROBIONET), CTQ2014-53334-C2-1-R. and MAT2015-71879-P). EMP acknowledges the European Research Council (ERC-PoC-842606), MINECO (CTQ2017-86060-P), Comunidad de Madrid (MAD2D-CM S2013/ MIT-3007). IMDEA Nanociencia acknowledges support from the 'Severo Ochoa' Programme for Centres of Excellence in R&D (MINECO, Grant SEV- 2016-0686). RdC acknowledges support from UAM, Banco Santander, Fundación IMDEA (convocatoria CRUE-CSIC-SANTANDER, fondo supera 2020, project with reference 10.01.03.02.41). Authors also acknowledge BAT unit of CIAL.

References

Alahi, M.E.E., Mukhopadhyay, S.C., 2017. Sensors 17(8).
Arcudi, F., Đorđević, L., Prato, M., 2016. Angew. Chem.-Int. Edit. 55(6), 2107-2112.
Catalán-Gómez, S., Briones, M., Cortijo-Campos, S., García-Mendiola, T., de Andrés, A., Garg, S., Kung, P., Lorenzo, E., Pau, J.L., Redondo-Cubero, A., 2020. Sci Rep 10(1), 16039.
Cesewski, E., Johnson, B.N., 2020. Biosens. Bioelectron. 159, 112214.
Chen, X., McGlynn, C., McDonald, A.R., 2018. Chem. Mat. 30(20), 6978-6982.
Díez Tascón, J.M., 2007. Opt. Pura Apl. 40(2), 149-159.
dos Santos, É., da Silva Martinho, H., Annes, K., da Silva, T., Soares, C., Ferreira Leite, R., Milazzotto, M., 2016. J. Biomed. Opt. 21(7), 075002.
Dutta, S., Dutta Chowdhury, A., Biswas, S., Park, E.Y., Agnihotri, N., De, A., De, S., 2018. Biochem. Eng. J. 140, 130-139.
Fan, X., Xu, P., Zhou, D., Sun, Y., Li, Y.C., Nguyen, M.A.T., Terrones, M., Mallouk, T.E., 2015. Nano Lett. 15(9), 5956-5960.
García-Mendiola, T., Cerro, M.R., López-Moreno, J.M., Pariente, F., Lorenzo, E., 2016. Bioelectrochemistry 111, 115-122.
García-Mendiola, T., Requena-Sanz, S., Martínez-Periñán, E., Bravo, I., Pariente, F., Lorenzo, E., 2020. Electrochim. Acta 353, 136522.
Gehring, A.G., Tu, S.-I., 2011. Annu. Rev. Anal. Chem. 4(1), 151-172.
Giovanelli, E., Castellanos-Gomez, A., Pérez, E.M., 2017. ChemPlusChem 82(5), 732-741.
Guerrero-Esteban, T., Gutiérrez-Sánchez, C., Martínez-Periñán, E., Revenga-Parra, M., Pariente, F., Lorenzo, E., 2021. Sens. Actuator B-Chem. 330, 129389.
Hunt, K., Vacelet, M., Jordan, K., 2017. Irish J. Agric. Food Res. 56(1), 25-30.
Jariwala, D., Sangwan, V.K., Lauhon, L.J., Marks, T.J., Hersam, M.C., 2014. ACS Nano 8(2), 1102-1120.
Jiang, Z., Zhao, C., Lin, L., Weng, S., Liu, Q., Lin, X., 2015. Anal. Methods 7(11), 4508-4513.
Jiang, K., Nie, D., Huang, Q., Fan, K., Tang, Z., Wu, Y., Han, Z. 2019. Biosens. Bioelectron. 130, 322-329.
Krzyszkowska, E., Walkowiak-Kulikowska, J., Stienen, S., Wojcik, A., 2017. Phys. Chem. Chem. Phys. 19(22), 14412-14423.
Law, J.W.-F., Ab Mutalib, N.-S., Chan, K.-G., Lee, L.-H., 2015. Front. Microbiol. 5(770).
Lazcka, O., Campo, F.J.D., Muñoz, F.X., 2007. Biosens. Bioelectron. 22(7), 1205-1217.
Li, H., Zhang, Q., Yap, C.C.R., Tay, B.K., Edwin, T.H.T., Olivier, A., Baillargeat, D., 2012. Adv. Funct. Mater. 22(7), 1385-1390.
Lin, M., Wan, H., Zhang, J., Wang, Q., Hu, X., Xia, F., 2020. ACS Appl. Mater. Interfaces 12(41), 45814-45821.
Liu, Y., Zhao, Y., Jiao, L., Chen, J. 2014. J. Mater. Chem. A. 2, 13109-13115.
Malorny, B., Tassios, P.T., Rådström, P., Cook, N., Wagner, M., Hoorfar, J., 2003. Int. J. Food Microbiol. 83(1), 39-48.
Marušić, A., 2011. J. Glob. Health 1(1), 72-78.
Nie, Y., Zhang, X., Zhang, Q., Liang, Z., Ma, Q., Su, X., 2020. Biosens. Bioelectron. 160, 112217.
Pang, D. W., Qi, Y. P., Wang, Z. L., Cheng, J. K., Wang, J. W., 1995. Electroanalysis. 7(8), 774-777.
Quirós-Ovies, R., Vázquez Sulleiro, M., Vera-Hidalgo, M., Prieto, J., Gómez, I.J., Sebastián, V., Santamaría, J., Pérez, E.M. 2020. Chem. Eur. J. 26, 6629-6634.
Rigodanza, F., Đorđević, L., Arcudi, F., Prato, M., 2018. Angew. Chem.-Int. Edit.57(18), 5062-5067.
Rohaizad, N., Mayorga-Martinez, C.C., Fojtů, M., Latiff, N.M., Pumera, M., 2021. Chem. Soc. Rev. 50(1), 619-657.
Scallan, E., Hoekstra, R.M., Angulo, F.J., Tauxe, R.V., Widdowson, M.-A., Roy, S.L., Jones, J.L., Griffin, P.M., 2011. Emerg. Infect. Dis 17(1), 7-15.
Tuxen, A., Kibsgaard, J., Gøbel, H., Lægsgaard, E., Topsøe, H., Lauritsen, J.V., Besenbacher, F., 2010. ACS Nano 4(8), 4677-4682.

Wang, Q.H., Kalantar-Zadeh, K., Kis, A., Coleman, J.N., Strano, M.S., 2012. Nat. Nanotechnol. 7(11), 699-712.
Wu, J., Chao, Y., Yu, Y., Chen, J., Zhang, C.,Gao, R., Mu, X.,Geng, Y., He, J., 2020. Sensors & Actuators B. Chemical 305, 127280-127287.
Yang, T., Chen, M., Kong, Q., Luo, X., Jiao, K., 2017. Biosens. Bioelectron. 89, 538-544.

Supporting Information

A MoS_2 platform and thionine-carbon nanodots for sensitive and selective detection of pathogens

Emiliano Martínez-Periñán [a‡], *Tania García-Mendiola* [a,b*‡], *Estefanía Enebral-Romero* [a], *Rafael del Caño* [a], *Mariano Vera-Hidalgo* [c], *Manuel Vázquez Sulleiro* [c], *Cristina Navío* [c], *Félix Pariente* [a], *Emilio M. Pérez* [c] *and Encarnación Lorenzo* [a,b,c*]

[a] Departamento de Química Analítica. Universidad Autónoma de Madrid. 28049 Madrid (Spain).

[b] Institute for Advanced Research in Chemical Sciences (IAdChem), Universidad Autónoma de Madrid, Ciudad Universitaria de Cantoblanco, 28049, Madrid (Spain).

[c] IMDEA-Nanociencia, Ciudad Universitaria de Cantoblanco, 28049, Madrid (Spain).

*Corresponding author: tania.garcia@uam.es, encarnacion.lorenzo@uam.es

‡ Both authors contribute equally to this work.

Experimental

Chemicals

Sodium chloride, sodium phosphate, double stranded calf thymus DNA (dsDNA), DNA oligonucleotides, L-arginine, 3,3′-diamino-N-methyldipropylamine, Thionine acetate salt, 1,4-Dithiothreitol (DTT) and all other chemicals used in this work were purchased from Merk. Dialysis membrane tubing cutoff in the range of 0.1-0.5 kDa was provided by Spectrum Laboratories. Bulk MoS_2 powder (<2 μm, 98%) was obtained from Merk. Analytical reagent grade 2-propanol was purchased from Scharlab chemicals. Water was obtained in a Milli-Q filtration station (Type 1, ultrapure water; 18.2 MΩ cm at 25 ºC). All solutions were prepared using water purified with a Millipore Milli-Q-System (18.2 MΩ cm).

DNA samples

Different DNA samples were used in this work. Calf thymus double stranded DNA (dsDNA), 25-base synthetic oligonucleotide sequences from the InIA gen of *Listeria*

monocytogenes bacteria and open reading frame sequence (ORF1ab) of SARS-CoV-2 virus. The calf thymus, and the 25 and 28-base oligonucleotide sequences used in this work were supplied by Sigma-Aldrich Co (Table 1 of the main manuscript).

Apparatus

A Cary Eclipse Varian spectrofluorimeter and a Thermo Scientific™ Multiskan™ GO spectrophotometer were used for fluorimetric and spectrophomotometric measurements, respectively. 96-well microplates were used for absorbance titrations and supplied by JET-BIOFIL.

For electrochemical measurements an Autolab PGSTAT 30 potentiostat from Eco-Chemie using the software package GPES 4.9 was used. A screen-printed electrode Connector (DropSens) was used as interface. Screen-printed Carbon electrodes (CSPEs) were supplied by DropSens (Spain). CSPEs integrate a carbon working, an Ag/AgCl pseudoreference and a carbon counter electrode. A home-made electrochemical cell was used for all the electrochemical studies.

A CEM Discover microwave system (Matthews (NC), USA) was used for Thi-CNDs synthesis.

Fourier transform infrared (FTIR) spectra were recorded from KBr pressed pellets of the solid material and precursors in the wavelength range 5000–500 cm^{-1} using a Brucker IFS60v spectrometer.

For transmission electron microscopy (TEM), Lacey carbon support film copper grids (400 mesh, Electron Microscopy Sciences) were used. Images were recorded with a JEOL JEM 2100 electron microscope.

UV-Vis spectra were recorded using a UV-1900 from SHIMADZU spectrophotometer using a quartz cell.

XPS (X ray Photoelectron Spectroscopy) measurements were performed under Ultra High Vacuum conditions (UHV, with a base pressure of 5×10^{-10} mbar), using a monochromatic Al Kα line as exciting photon source for core level analysis (hν = 1486.7 eV). The emitted photoelectrons were collected in a hemispherical energy analyzer (SPHERA-U7, pass energy set to 20 eV for the XPS measurements to have a resolution of 0.6 eV) and to compensate the built-up charge on the sample surface it was necessary the use of a Flood Gun (FG-500, Specs), with low energy electrons of 3 eV and 40 μA.

For the binding energy correction, two calibrations were used: the C 1s at 285.0 eV for the CSPEs electrodes and Au $4f_{7/2}$ at 84.0 eV for the Au electrodes.

Raman spectroscopy measurements were recorded on a Bruker Senterra confocal Raman microscope (Bruker Optic, Ettlingen, Germany, resolution 3–5 cm^{-1}) by using the following parameters: objective NA 0.75, 50X; laser excitation: 532 nm, 2 mW. Each spectrum results from the average of 3 measurements carried out in different regions distributed all over the sample. Optical microscope images were carried out using an Olympus microscope with a 50x objective lens.

SEM images of the electrodes were characterized working on a low voltage (2.5 kV) and current (10 pA) mode to avoid any damage of the sample by using a FESEM Auriga, Carl Zeiss equipped with an energy-dispersive X-ray spectrometer.

Atomic Force Microscopy (AFM) were acquired in a Ntegra Prima AFM system in semicontact mode. Rectangular silicon cantilevers HA_NC (NT-MDT) were used with typical values of 5.1 N·m–1 spring constant and 140 kHz resonant frequency. The images were processed using Gwyddion software.

X-ray diffraction (XRD) measurements were carried out using a Panalytical X'Pert PRO theta/2theta diffractometer with Cu-Kα radiation (λ= 0.1541 nm).

DNA stock solutions preparation

Double-stranded calf thymus DNA (dsDNA) stock solutions (1.0 mg mL^{-1}) were prepared in water. The concentration in base pairs (bp) of DNA was determined by using the molar absorptivity (6600 L mol^{-1} cm^{-1}) of DNA at 260 nm. Single stranded calf thymus DNA (ssDNA) was obtained by boiling in water vials containing dsDNA for 30 minutes and subsequently cooling them in an ice-bath and stored frozen at -20ºC.

Prior to use, stock solutions of *Listeria and* SARS-CoV-2 thiol-modified probe ($Probe_{List}$-SH and $Probe_{CoV}$-SH) were treated with DTT and then purified by elution through a NAP-10 column of Sephadex G-25. Afterwards, the stock solution of the thiolated probes was prepared at a concentration of 10.0 µM and 8.15 µM in 10 mM phosphate buffer (PB) pH 7.0, for the bacteria and virus, respectively. The stock solution of the analyte sequences ($Listeria_C$, $Listeria_{NC}$, CoV_C, $CoV_{NC,}$ and E. Coli) were prepared using 10 mM phosphate buffer (pH 7.0) with 0.4M NaCl as solvent. Aliquots of a few microliters of all stock solutions were stored at -20 ºC.

MoS_2 flakes preparation

In a round-flask of 250 mL volume, 150 mg of bulk MoS_2 was dispersed in 150 mL of 2-propanol and water (7:3 volume mixture). (Giovanelli et al., 2017) The mixture was cooled down at 2.5 ºC in a Minichiller Hubber and sonicated during an hour using an ultrasonic probe (Vibracell 75115, Bioblock Scientific, 500 W) with an amplitude of 40%. After sonication, the black suspension was transferred to six 50 mL conical centrifuge tubes and centrifugated in an Allegra X-15R Beckman Coulter centrifuge (FX6100 rotor, 20ºC) during 30 minutes at 1792 g (4000 rpm). The olive-color supernatant was carefully decanted from the black sediment and collected in a conical centrifuge tube for further experiments.

Bacterial culture and genomic DNA extraction and purification

Genomic DNA was extracted from the cultured Listeria monocytogenes. Firstly, 50 µL of *Listeria monocytogenes* bacterial strains were streaked on brain heart infusion (BHI) with 25% glycerol and incubated at 37.0 °C for 24 h. Then, 1 mL of each bacterial culture suspension was used for DNA extraction using the E.Z.N.A Bacterial DNA kit (Omega Bio-TEK) according to the manufacturer's instructions. A unique type of cell colony with a positive growth was obtained in purity test. The concentration of the obtained genomic DNA was measured using a NanoDrop spectrophotometer and then it was then stored at − 20 ◦C.

The bacterial colony-forming unit (CFU mL^{-1}) values or concentration of *Listeria monocytogenes* was measured by plate counting and found to be $(1.0 \pm 0.2) \times 10^9$ CFU mL^{-1} or 313 ng μL^{-1} of total DNA and 2.70 pg μL^{-1} (3.48 nM) of the specific sequence of gen InIA (0.0087% of the total DNA). As a control, a genomic DNA sample cultured from *Lactobacillus rhamnosus* and extracted using the same procedures described above was used in order to assess the selectivity of the developed biosensor.

Listeria monocytogenes and *Lactobacillus rhamnosus* genomic DNA samples were denatured by boiling in water capped vials containing the samples for 30 minutes followed by rapid cooled. To prevent spontaneous renaturalization, this solution was subsequently quenched in an ice-bath. Finally, 10 µL of denatured sample were diluted to a final volume of 60 µL with 10 mM phosphate buffer (pH 7.0) with 0.4 M NaCl. The final total DNA concentration in this diluted sample was of 52.0 ng μL^{-1}(1.67×10^8 CFU

mL^{-1}) determined with the NanoDrop spectrophotometer, which corresponds to 0.45 pg μL^{-1}or 0.58 nM of a sequence of InIA gen.

Interaction between DNA and Thi-CNDs

Spectroscopic titrations

Absorbance and photoluminescence (PL) titrations of Thi-CNDs and DNA were carried out fixing Thi-CNDs concentration (0.280 mg mL^{-1}) and varying the concentration of dsDNA and ssDNA from 10.0 µM to 200 µM. Purified water or 0.1 M phosphate buffer (PB) pH 7.0 were used as solvent. All solutions were left to incubate for about 30 minutes before measuring.

The absorbance was plotted *vs.* DNA concentration in base pairs. Following the equation 1 described by Becker y Meehan (Meehan et al., 1982), the intrinsic binding constants, K_b, were determined:

$$[ADN] / (\varepsilon_a - \varepsilon_f) = [ADN] / (\varepsilon_b - \varepsilon_f) + 1 / K_b (\varepsilon_a - \varepsilon_f) \qquad \text{Equation 1}$$

where ε_a is the molar absorptivity of Thi-CNDs in presence of the different concentrations of DNA and ε_f and ε_b are the molar absorptivity of free and bound forms of Thi-CNDs, respectively.

The interaction strength was also quantified from PL titrations using the equation 2, similar to Stern-Volmer equation (Paul and Suresh Kumar, 2012):

$$(I_o - I)/I = K [DNA] \qquad \text{Equation 2}$$

The constants were calculated from the I_o/I vs. [DNA] plot, where I_o and I are the fluorescence intensity of the free and the bound Thi-CNDs to DNA, respectively.

Cyclic voltametric studies

Carbon screen-printed disposable electrodes (CSPE) were used for electrochemical measurements. Firstly, CSPE surfaces were cleaned with water and modified with DNA by drop casting 10 µL of a solution of 1.0 mg mL^{-1} ds or ssDNA (ds-ssDNA/ CSPE). Then the solution drop was allowed to evaporate for 24 hours at room temperature and the DNA modified electrode was rinsed with Milli-Q water to remove unabsorbed

material. Finally, the electrodes were immersed in a 0.280 mg mL^{-1} Thi-CNDs solution and cyclic voltammograms (CV) were carried out.

Results and discussion

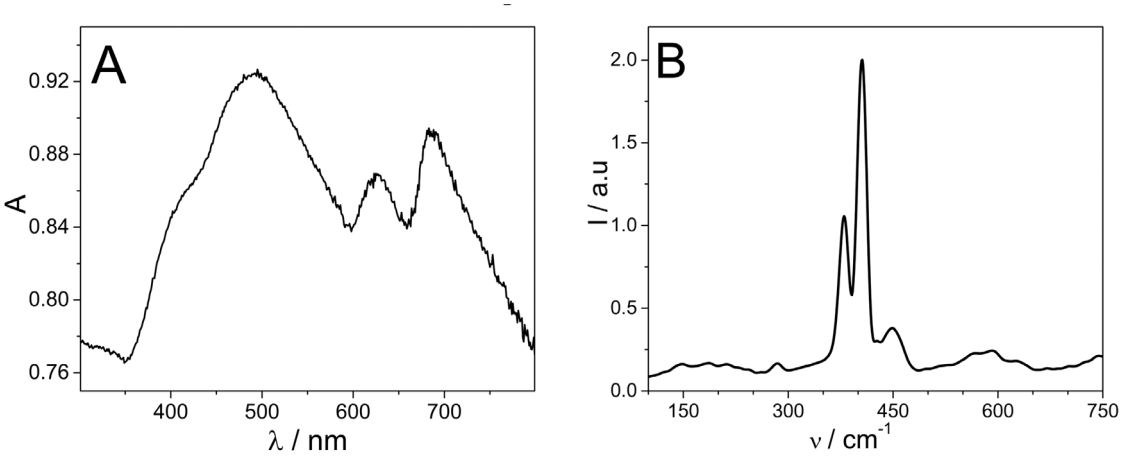

Figure S1. (A) UV-Vis spectrum of exfoliated MoS_2 in 2-propanol/water (7:3; v/v). (B) Raman spectrum (laser excitation 532 nm) of exfoliated MoS_2 powder.

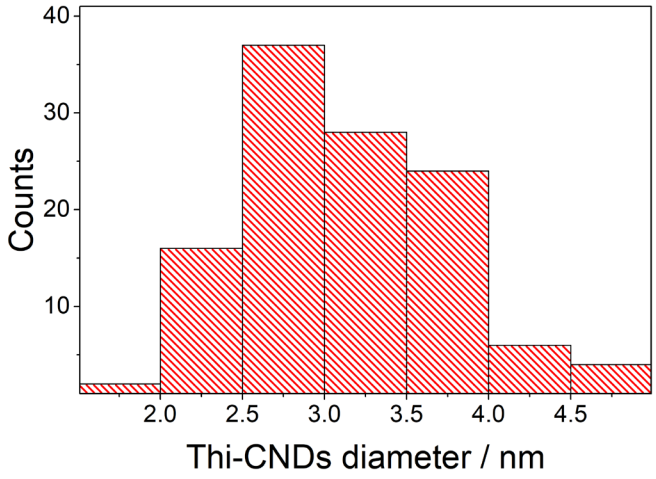

Figure S2. Thi-CNDs diameter histogram obtained by TEM from the measurements of around 120 Thi-CNDs.

DNA and Thi-CNDs Interaction

Spectroscopic studies

It is well known that the interaction of small molecules with DNA can induce changes in their electronic spectrum. Based on these changes, one can elucidate the type of interaction (Breslin et al., 1997). Hence, we recorded the UV-visible spectra of Thi-CNDs

in absence and in the presence of increasing amounts (from 30.0 μM to 200 μM) of dsDNA or ssDNA in water or in 0.1 M phosphate pH 7.0 (Figure S3 A, B). The absorption spectra of Thi-CNDs in pure water upon addition of increasing concentrations of dsDNA or ssDNA show a progressive absorbance decrease or hypochromic effect in the absorption maximum of Thi-CNDs centered at 600 nm, as well as a slight shift towards higher wavelengths (bathochromic effect). These effects are more accused in the case of dsDNA. The DNA-induced spectral variations observed can be explained in terms of changes in the local polarity around the chromophore, due to strong interactions with pyrimidine and purine bases (Pyle et al., 1989) and confirm a strong interaction between Thi-CNDs and DNA. From the absorption spectra changes, we estimated the respective binding constants. These values can be used to quantify the strength of interaction. According to Equation 1 (see experimental section SI), the intrinsic binding constants (K_b) were found to be 7.05 10^5 M^{-1} and 1.40 10^4 M^{-1} for ds and ssDNA, respectively. These values are similar to those reported in the literature for compounds that strongly interact with DNA through intercalation (Bai et al., 2004). Moreover, the difference in the binding constant for ds and ssDNA suggests that Thi-CNDs has a higher affinity to dsDNA. In order to further investigate this interaction, we also evaluated the effect of other parameters that may affect the mode of interaction, in particular the increase of the ionic strength using 0.1 M PB as solvent instead of water. The electronic spectra of Thi-CNDs, in absence and in presence of ds or ssDNA, in 0.1 M PB pH 7.0 (Figure S3 C, D) were recorded and the binding constants for dsDNA and ssDNA were calculated. Values of 2.00 x 10^5 M^{-1} and 1.00 x 10^4 M^{-1}, respectively, were found. These values are quite similar to those obtained in pure water, suggesting that the increase of the ionic strength (using phosphate solution) do not affect the interaction, which indicates that it is probably mainly by intercalation between the base pairs rather than electrostatic.

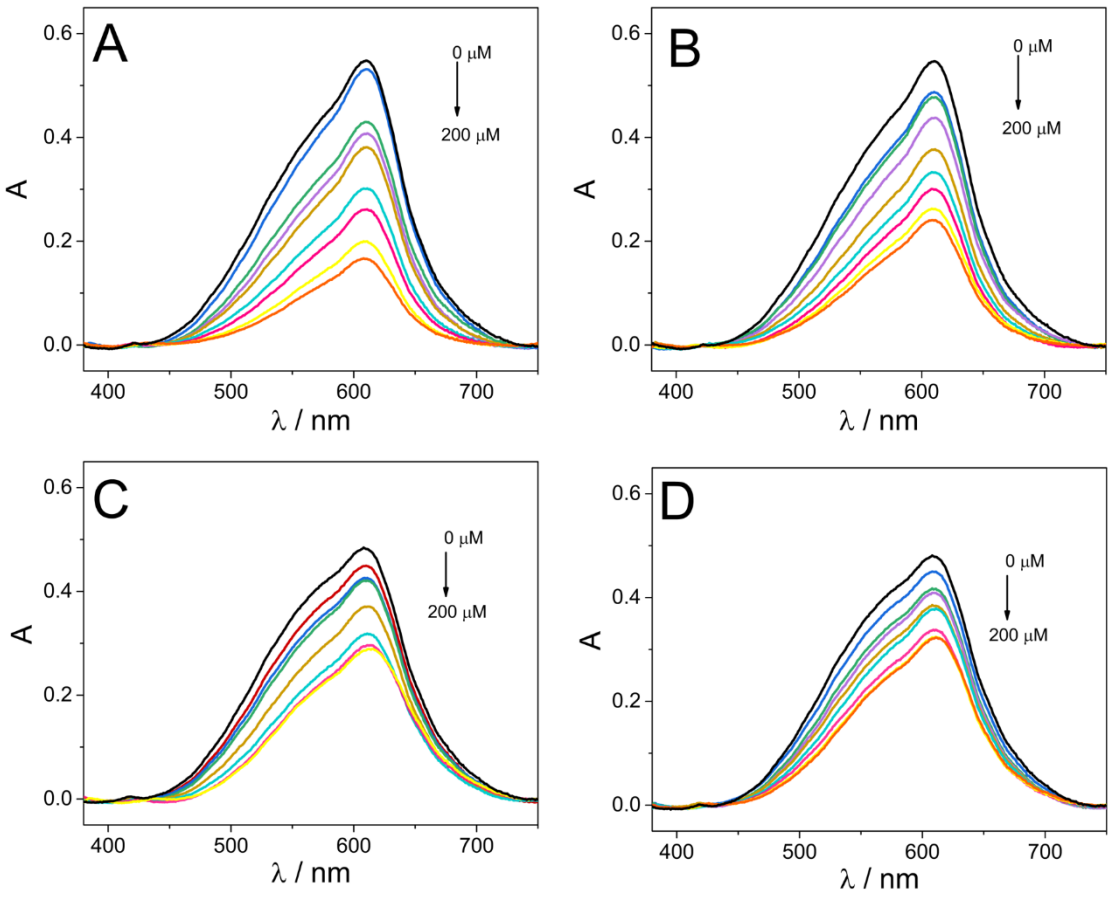

Figure S3. Absorption spectra of Thi-CNDs in the absence (black line) and in the presence of increasing amounts of dsDNA (A, C) or ssDNA (B, D) in water (A,B) and in 0.1 M PB pH 7.0 (C,D).

The Thi-CNDs show photoluminescence with a maximum centred at 355 nm, when they are excited at 300 nm. As in the case of absorption bands, we have exploited this property for studying their interaction with ds and ssDNA. For this purpose, the emission spectra of the Thi-CNDs in the absence and in the presence of increasing amounts of ds or ssDNA were recorded. The addition of DNA (Figure S4) gives rise to a gradual increase in the emission intensity. This effect has been reported for molecules binding to DNA via an intercalative mode (Fritzsche et al., 1982). From the fluorescence spectra changes, we also estimated the interaction strength between the Thi-CNDs and DNA. The binding constants (calculated as described in experimental section) were found to be 1.05 x 10^4 and 5.20 x 10^3 M^{-1} for ds and ssDNA, respectively. These values confirm the stronger interaction of dsDNA and are similar to those reported for other molecules.

The above results point out to a strong interaction between the Thi-CNDs and DNA, being stronger with ds than with ssDNA.

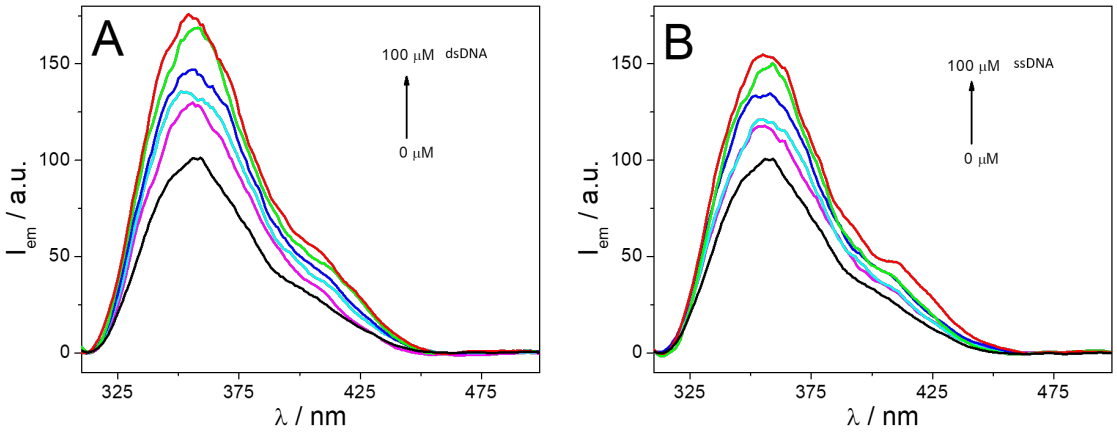

Figure S4. Emission spectra of Thi-CNDs in the absence (black line) and in the presence of increasing amounts of dsDNA (A, C) or ssDNA (B, D) in water.

Electrochemical behaviour of Thi-CNDs at DNA-modified electrodes.

With the aim of corroborating the results obtained above and based on Thi-CNDs electroactivity, we carried out electrochemical studies to analyze their interaction with DNA and their potential application as an electrochemical indicator of the hybridization event in the development of electrochemical biosensors. For these studies, we employed carbon screen printed electrodes (CSPEs) as drop-on sensors in order to further develop portable DNA sensing devices. DNA modified electrodes are not only useful for studying the interactions of DNA with other molecules, but also for their application to the development of biosensors.

Figure S5 shows the CV response of Thi-CNDs at ds or ssDNA/CSPE (curves b, red and c, blue), using 0.1 M PB pH 7.0 solution as supporting electrolyte. At dsDNA/CSPE, it can be seen the two characteristic redox peaks ascribed to the oxidation/reduction of the Thi-CNDs but shifted to more positive potentials ($E^{o\prime}$ values of -0.30 and -0.40 V). Moreover, an increase in the peak current and a decrease in ΔEp compared to CV obtained at bare CSPE (curve a, black) are observed. Similar results were obtained for ssDNA/CSPE, but in this case the peak at around -0.40 V is poorly defined. Both, the increase in the peak currents and the shift in the formal potentials ($E^{o\prime}$) towards more positive potential are less accused than in the case of dsDNA. These results are consistent with a strong interaction by intercalation between Thi-CNDs and DNA immobilized on the electrode surface (Pang and Abruña, 1998; Pang et al., 1995) and agree well with those obtained by spectroscopic techniques, confirming that the interaction with dsDNA is stronger than with ssDNA. In addition, in both cases (ss and dsDNA/CSPE) the peak

current was directly proportional to the scan rate, ν, which is characteristic of a surface-confined redox process. Furthermore, as can be observed in Figure S5 B, after repetitive potential cycles, there is an increase in the peak current confirming the accumulation of Thi-CNDs in the immobilized dsDNA layer. If after repetitive cycles, the electrode is removed from the cell, rinsed with water, and placed in fresh electrolyte solution containing no Thi-CNDs, a voltammetric response typical of redox couples confined at the electrode surface is observed for the dsDNA/CSPE, ssDNA/CSPE and CSPE (data not shown). This response is ascribed to the oxidation of the Thi-CNDs accumulated on the electrode surface or in the DNA layer, being higher when the electrode is modified with the dsDNA. Differential Pulse voltammetry allows a better discrimination between overlapped redox processes besides a high sensitivity. Hence, we recorded the Differential Pulse Voltammogram (DPV) of Thi-CNDs accumulated on the electrode surface (see Figure S6). It confirms that the incorporated Thi-CNDs remains tightly bound to the DNA layer and in the case of dsDNA/CSPE, the peak current is much higher than in the case of ssDNA /CSPE or CSPE, suggesting again a stronger interaction with the dsDNA.

The results presented above point to the utility of Thi-CNDs as electrochemical indicator of the hybridization event in the development of a DNA biosensor.

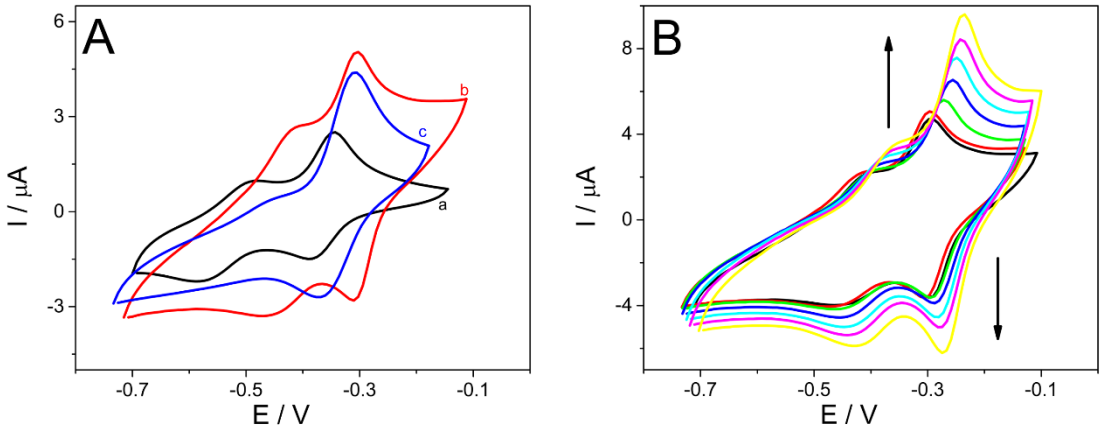

Figure S5. (A) Cyclic voltammograms of Thi-CNDs in 0.1 M PB pH 7.0 solution at a bare CSPE electrode (a, black curve) and at a dsDNA/CSPE electrode (b, red curve) and at a ssDNA/CSPE (c, blue curve). Scan rate: 100 mV s^{-1}. (B) Consecutive cyclic voltammograms of Thi-CNDs at a dsDNA/CSPE in 0.1 M PB pH 7.0. Scan rate: 100 mV s^{-1}.

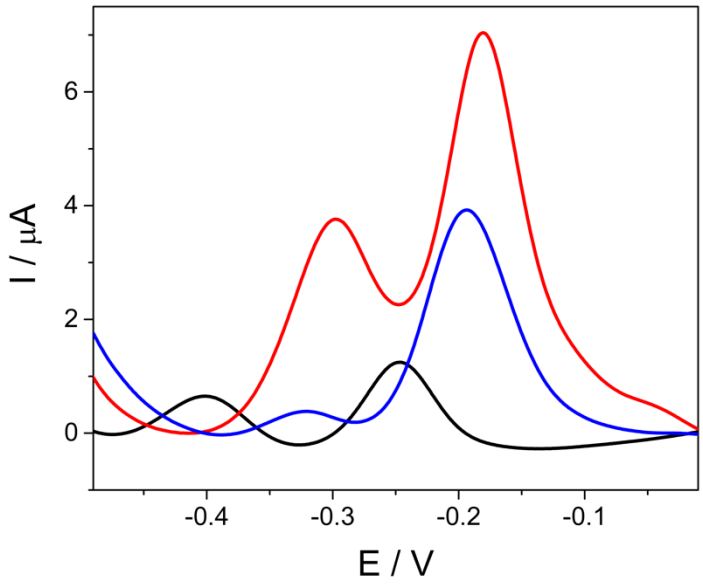

Figure S6. DPVs of Thi-CNDs in in 0.1 M PB pH 7.0 after accumulation in CSPE (black curve), ssDNA/CSPE (blue curve) and dsDNA/CSPE (red curve).

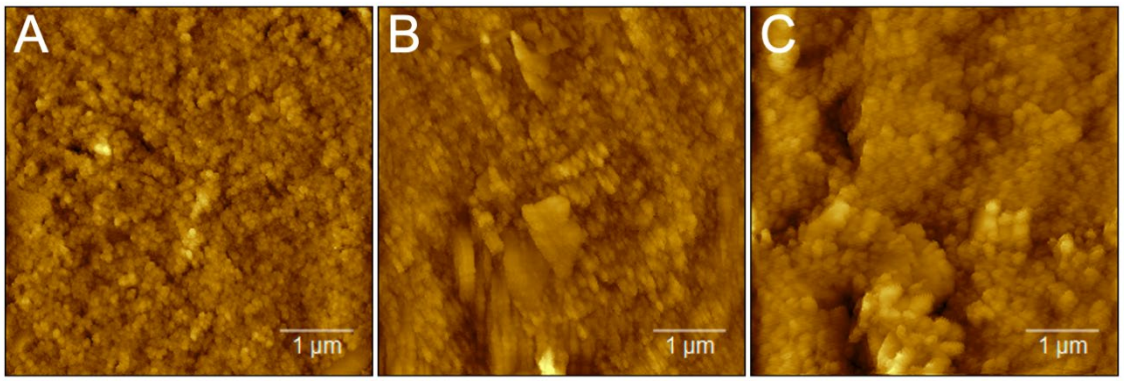

Figure S7. 5 x 5 µm AFM images of (A) CSPE (B) MoS_2/CSPE and (C) Probe-SH/MoS_2/CSPE.

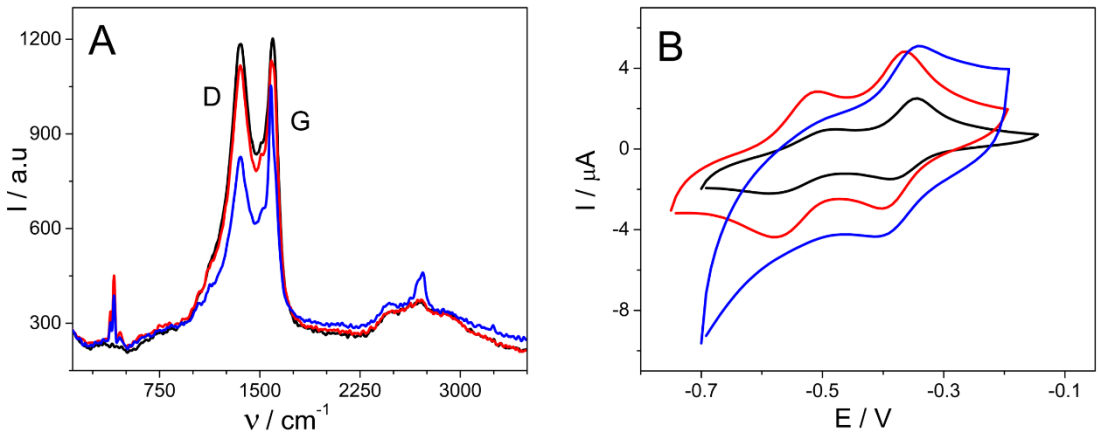

Figure S8. Raman spectrum (A) of a CSPE (black curve), MoS_2/CSPE (red curve) and Probe-SH/ MoS_2/CSPE (blue curve). B) Cyclic voltammograms of Thi-CNDs in 0.1 M PB pH 7.0 solution at a bare CSPE electrode (black curve), a MoS_2/CSPE (red curve) and a Probe-SH/MoS_2/CSPE (blue curve). Scan rate: 100 mV s^{-1}.

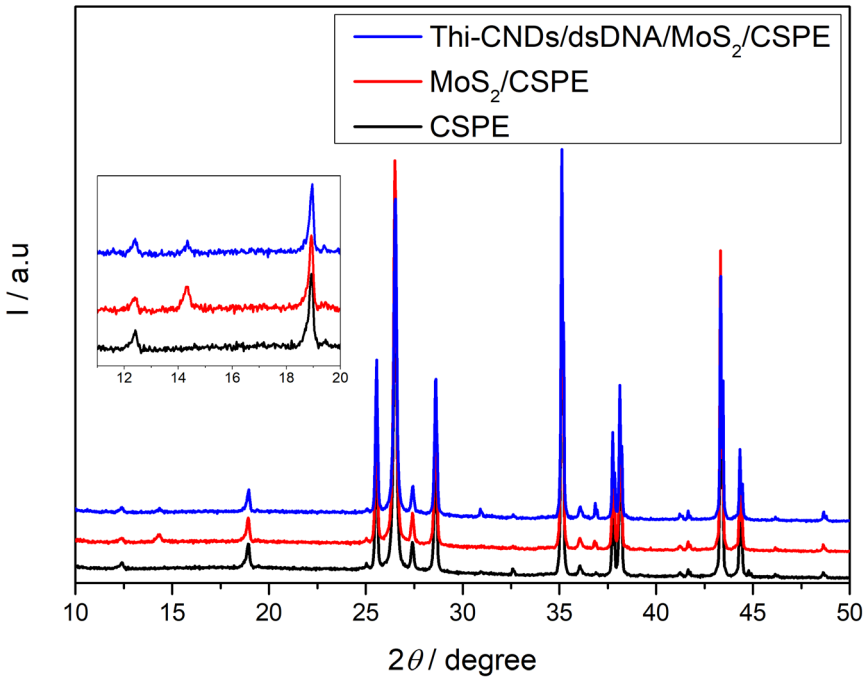

Figure S9. XRD patterns of CSPE (black), MoS_2/CSPE (red) and Thi-CNDs/dsDNA/MoS_2/CSPE (blue).

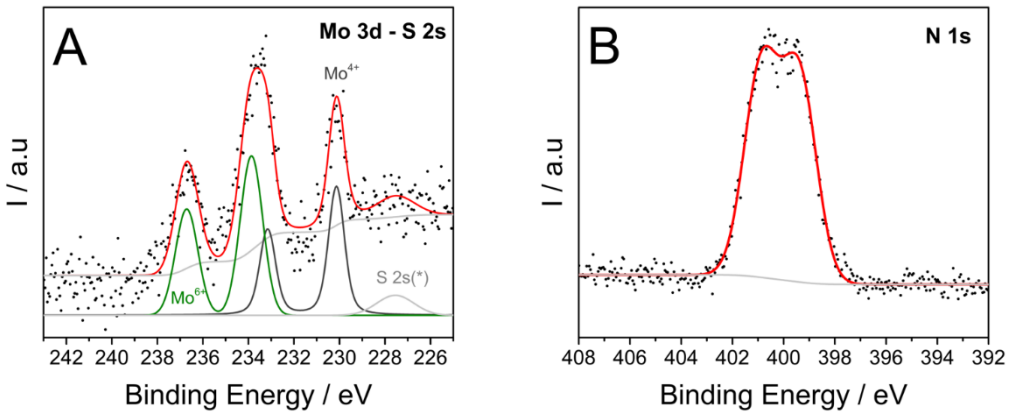

Figure S10. XPS *core levels* of the region of Mo 3d showing the presence of MoS_2 (A) and N 1s from the DNA anchored to the MoS_2/CSPE electrode(B).

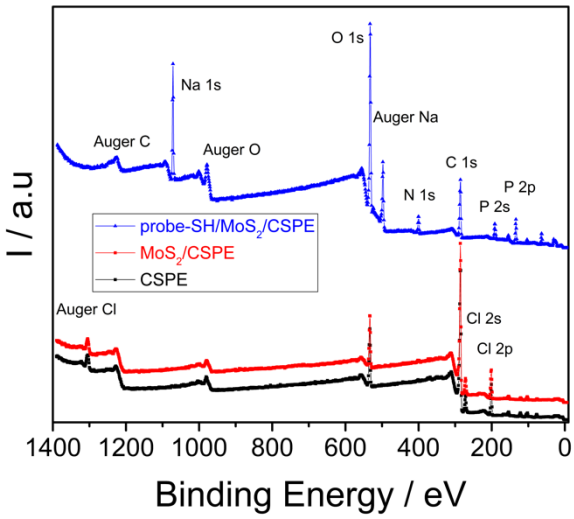

Figure S11**.** XPS survey spectra of a CSPE (black line), MoS_2/CSPE (red line) and probe-SH/ MoS_2/CSPE (blue line).

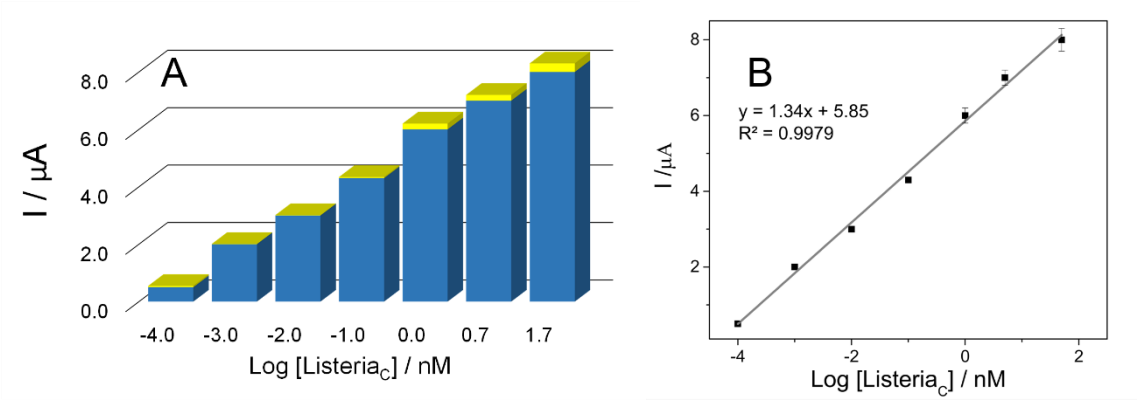

Figure S12**.** A) Bar diagrams of the biosensor response before and after the hybridization with increasing concentrations of the analyte sequence, Listeria$_C$ (from 100 fM to 50.0 nM). B) Calibration plot with values obtained from 3 determinations.

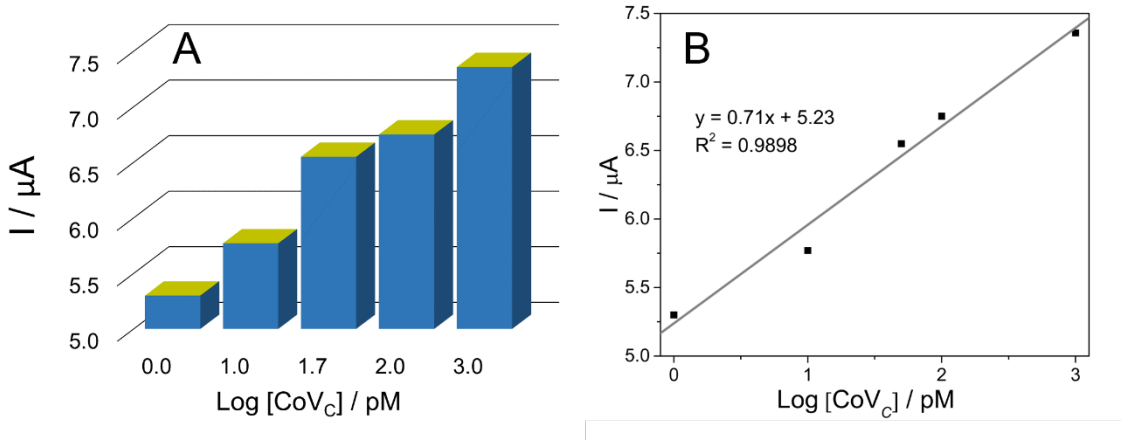

Figure S13. A) Bar diagrams of the biosensor response before and after the hybridization with increasing concentrations of the analyte sequence, CoV$_C$ (from 1.00 pM to 1.00 nM). B) Calibration plot with values obtained from 3 determinations.

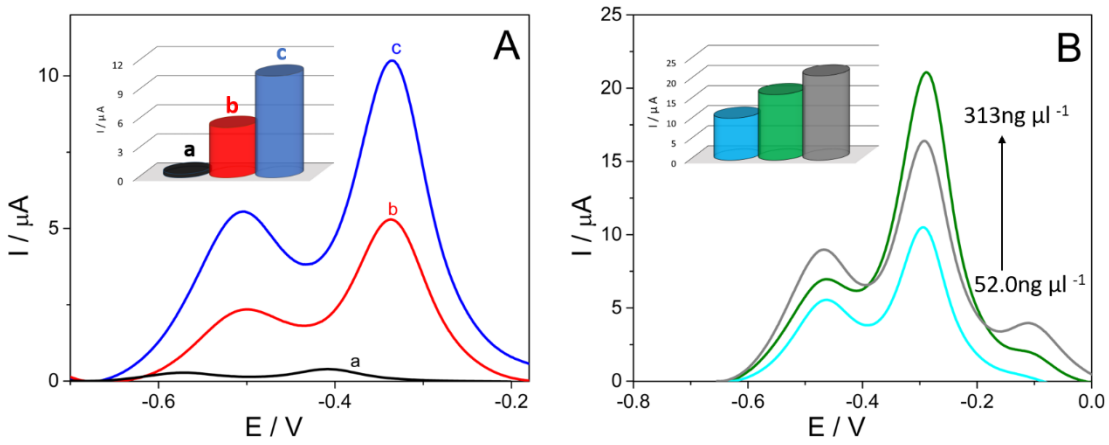

Figure S14. DPVs and bar diagrams (insets) of the peaks current of Thi-CNDs accumulated on a $Probe_{LIST}$-SH/ MoS_2/ CSPE in PB 0.1M pH 7.0: A) before (a, black curve) and after hybridization with genomic DNA samples extracted from cultured *Listeria monocytogenes* (c, blue curve) and genomic DNA samples extracted from *Lactobacillus rhamnosus*, used as a control (b, red curve), B) after hybridization with increasing amounts (from 52.0 to 313 ng μL^{-1}) of genomic total DNA extracted from cultured *Listeria monocytogenes*.

Table S1. Comparative biosensors for pathogens detection.

Target Pathogen	Based on	Method	L.O.D	Reference
Hepatitis B virus	ZnO (NPs)/MoS_2 NWs	FET	1fM	Shariati et al., 2021
HPV 16 DNA	Zn-doped MoS_2 / QDs/ Cu(I)NPs	ECL	0.03 nM	Nie et al., 2020
Hepatitis C virus (HCV)	BN QDs/MoS_2	ECL	0.17 pM	Liu et al., 2020
Aflatoxin B1 (AFB1)	DNA/MoS_2–AuNPs	DPV	0.01 fg/mL	Peng et al., 2018

References

Bai, G.-Y., Dong, B., Lü, Y.-Y., Wang, K.-Z., Jin, L.-P., Gao, L.-H., 2004. J. Inorg. Biochem. 98(12), 2011-2015.

Breslin, D.T., Yu, C., Ly, D., Schuster, G.B., 1997. Biochemistry 36(34), 10463-10473.

Fritzsche, H., Triebel, H., Chaires, J.B., Dattagupta, N., Crothers, D.M., 1982. Biochemistry 21(17), 3940-3946.

Giovanelli, E., Castellanos-Gomez, A., Pérez, E.M., 2017. ChemPlusChem 82(5), 732-741

Liu, Y., Nie, Y., Wang, M., Zhang, Q., Ma, Q., 2020. Biosens. Bioelectron. 148, 111823.

Meehan, T., Gamper, H., Becker, J.F., 1982. J. Biol. Chem. 257(17), 10479-10485.

Nie, Y., Zhang, X., Zhang, Q., Liang, Z., Ma, Q., Su, X., 2020. Biosens. Bioelectron. 160, 112217.

Pang, D.-W., Abruña, H.D., 1998. Anal. Chem. 70(15), 3162-3169.

Pang, D.-W., Qi, Y.-P., Wang, Z.-L., Cheng, J.-K., Wang, J.-W., 1995. Electroanalysis 7(8), 774-777.

Paul, P., Suresh Kumar, G., 2012. J. Fluoresc. 22(1), 71-80.

Peng, G., Li, X., Cui, F., Qiu, Q., Chen, X., Huang, H., 2018. ACS Appl. Mater. Interfaces. 10(21), 17551-17559.

Pyle, A.M., Rehmann, J.P., Meshoyrer, R., Kumar, C.V., Turro, N.J., Barton, J.K., 1989. J. Am. Chem. Soc. 111(8), 3051-3058.

Shariati, M., Vaezjalali, M., Sadeghi, M., 2021. Anal. Chim. Acta. 1156, 338360.